Measuring cell density in an acoustofluidic micro-cavity

line 1: 1st Harrisson D. A. Santos
line 2: Physical Acoustics Group
line 3: Federal University of Alagoas
line 4: Maceió, Brazil
line 5: hdasantos@fis.ufal.br

line 1: 2st Giclênio C. Silva
line 2: Physical Acoustics Group
line 3: Federal University of Alagoas
line 4: Maceió, Brazil
line 5: email address or ORCID

line 1: 3st Tiago F. Vieira
line 2: Institute of Computing
line 3: Federal University of Alagoas
line 4: Maceió, Brazil
line 5: email address or ORCID

line 1: 4th Amanda E. Silva
line 2: Laboratory of Pharmacology
line 3: Federal University of Alagoas
line 4: Maceió, Brazil
line 5: email address or ORCID

line 1: 5st Ícaro B. Q. de Araújo
line 2: Institute of Computing
line 3: Federal University of Alagoas
line 4: Maceió, Brazil
line 5: email address or ORCID

line 1: 6st Carlos Jacinto
line 2: 4Nanophotonics and Images Group
line 3: Federal University of Alagoas
line 4: Maceió, Brazil
line 5: email address or ORCID

line 1: 7st Ueslen Rocha
line 2: 4Nanophotonics and Images Group
line 3: Federal University of Alagoas
line 4: Maceió, Brazil
line 5: email address or ORCID

line 1: 8st Magna S. Alexandre-Moreira
line 2: Laboratory of Pharmacology
line 3: Federal University of Alagoas
line 4: Maceió, Brazil
line 5: email address or ORCID

line 1: 9st Glauber T. Silva
line 2: Physical Acoustics Group
line 3: Federal University of Alagoas
line 4: Maceió, Brazil
line 5: gtomaz@s.ufal.br

***Abstract*— Detecting changes in the density of biological cells is of paramount importance as it may reveal the cell status in processes such as differentiation and disease. An ideal methodology for measuring density would fastly screen the mass and volume of individual cells in a population, allowing the cells to be taken for further analysis. To achieve this goal, we introduce a 3D printed acoustofluidic levitation device to quantify single-cell density and volume with high accuracy/**

INTRODUCTION

Acoustofluidics is prescribed as a combination of acoustic fields propagating in a fluidic medium bounded in a micro-to-nanoscale container.[1] Particles suspended in the fluidic medium can be selectively manipulated under the action of these acoustic fields. [2] This selective manipulation can be used for trapping microparticles who share similar mechanical and physical properties such as cells of a specific cellular family. Regarding bioapplications, acoustofluidics cover a huge range by offering point-care and life-science devices for many applications such as tissue engineering,[3] infectious diseases,[1, 4] cancer cells [5] etc.

At the acoustofluidic field, the device's technology is a label-free, biocompatible, and contactless platform for diagnosis in cells' assays that can be coupled with other requirements to mimic the living-cells conditions during the experiments. These devices do not work only on their own but also work hand in hand with other techniques proposed for disease diagnosis. For example, we have reported recently a 3D printed acoustofluidic prototype proffering assistance for Raman biospectroscopy, especially for reducing/avoiding spurious background signal from the surroundings.[6] The purpose of the quoted study was to provide an improved platform based on Raman-acoustofluidics for reading cellular structure of a cell and seeking for information of its state.

Still concerning bioapplications, the density of a cell is one of the key features for providing information of changes in its internal cellular structure. In despite of this, there are few methodologies proposed for such a task.[7, 9] For this reason, we proposed a 3D-printed acoustofluidic levitation device to measure the density of micro-objects such as a cell of macrophage line j774.A.1

Experimental methodology

Cell preparation

The adherent-phenotype macrophage line j774.A1 was cultured in Dulbecco's Modified Eagle's Medium (DMEM, Merck KGaA, Germany) supplemented with 10% FBS at 37 °C, 95% humidity and 5% CO2. Cells are cultured to 90% confluence and later centrifuged at 1500 rpm for 5 min at 4°C to separate dead cells from living cells. Subsequently, the living cells were counted using an optical microscope and a Neubauer's chamber. For the cell weighing experiment, we used $1x10^2$ cells inside of the device.

Acoustofluidic Device Fabrication

The acoustic trapping of microparticles or cells was performed in a cylindrical acoustic chamber with a height of H = 750 μm and diameter of 2R = 4mm. The chamber was cast inside a cylindrical disk, which was fabricated with a 3D printer (Moonray D75, 24 Sprintray, Inc., USA) through the digital light-processing technique. A piezoceramic actuator (lead zirconate titanate, PZT-8) with a diameter of 25mm was glued with epoxy (Huntsman Corp., USA) as the bottom of the resonant chamber. A glass cover slide of 150 μm thickness was glued at the chamber's top, working as an acoustic reflector. In Fig. 1, the acoustofluidic device is shown.

Protocol to achieve single-cell measurements

The number of cells (or polystyrene beads) introduced inside the cavity for our measurements was about $1x10^2$ cells (polystyrene beads).There are some acoustic phenomena

inside the cavity that promotes a particle-to-particle interaction, which, in turns, induces a package of agglomerated particles. In order to achieve a single-particle configuration, we switched off the device once an assembly of particles started to form. After that, about 10 seconds later, we turned on the device again, and only a single-particle settled at the pressure node. We could repeat this procedure several times, with a good rate of success.

Results and discussion

Fig. 1(a) presents an optical photo of our system proposed for weighing scales of cells (and/or micro-objects). A 3D printed acoustofluidic device mounted on a confocal microscope composes the system. The confocal microscope provides bright optical images of the micro-objects for the methodological analyses. A set of components compose the acoustofluidic device as shown in Fig. 1(b). The acoustic-resonator chamber is cast inside the cylindrical disc constituted by the resin material described in the experimental section. The top and the bottom parts of the chamber have as frontiers a microscope coverslip and a piezoceramic transducer (PZT) substrate. The first is well-suitable for optical confocal microscopy and works as an acoustic reflector. The PZT is responsible for the generation of acoustic waves inside the resonator cavity. The lateral walls of the microfluidic cavity is based on resin material. Fluidic solutions of cells (and micro-particles, in general) can be introduced inside the resonator cavity by an inlet (left hand from the cavity) and, after finishing experiments, removed by an outlet channel (right hand from the cavity), see better in the cross-section cut view of the device presented in Fig. 1(c).

Inside of the resonator cavity, the acoustic waves of 1.034 MHz are produced by the PZT when an electrical voltage is applied to it. Fig. (d) pictures the case of non-establishments of acoustic waves, which means that there is no voltage applied. For this case, when we introduce a solution of cells inside the cavity by the inlet channel, the cells just fall to the bottom of the chamber. On the other hand, as the voltage supply is turned on, a standing acoustic wave is established inside the well-sealed resonator cavity (Fig. 1(e)). An acoustic radiation force acts on the cells to deliver and handle them to be levitated and trapped at the pressure node. For the case of our experimental purpose, a methodology was applied to keep only a single-cell at the pressure node.

The single-cell trapped at the pressure node, is levitating in a height $h \sim 95\ \mu m$ from the bottom of the cavity. We used a 40X objective lens (NA = 0.65) of 600 μm working distance, which can be adjusted to well match its light confocal plane to the acoustic levitation plane. By doing so, the cell can be visualized, in real time and in a focused manner, by optical microscopy inspection. By matching the light confocal and the levitation plane we perform a first step of our methodology applied for measuring single-cell (or any single-microparticle) density. This situation is well pictured in Fig. 2(a). Focused bright-field images of a single-cell of macrophage (J774.A1) as well as a single-particle of polystyrene are shown in Fig. 2(c) (the frames correspond to the second and first line of the first column, respectively). The reason for using polystyrene particles is that the density of this material is well-know ($\rho \sim 1050\ kgm^{-3}$) and provided by Sigmaaldrich Company responsible for their fabrication.

An attempt to describe the second step is illustrated in Fig. 2(b). As we moved-up the objective lens, the bright-field images started to blur. This blurring (or defocusing) effect is observed by looking the cell's images, in second line in the Fig. 2(c), from the left (first column, indicated by the nomenclature $H_{rel} = 95\ \mu m$) to the right (second and third columns, indicated by $H_{rel} = 87$ and $79\ \mu m$). The nomenclature H_{rel} is associated with a relative height, defined as:

$$H_{rel} = 95\ \mu m - D \tag{1}$$

D is the relative distance between the levitation plane and the light confocal plane. As larger is the relative distance D more defocused becomes the cell's image. In addition, we can see from the images, along with the blurring effect, there is an enlargement of the cells' size in the image. Fig. 2(d) shows the relative height H_{rel} as a function of a relative area A_{rel} of the cell in the bright-field image (green data). The relative area A_{rel} is defined by:

$$A_{rel} = \frac{Area(H_{rel}) - Area(95\mu m)}{Area(79\mu m) - Area(95\mu m)} \tag{2}$$

$Area(H_{rel})$ is the measured area of the cell in the bright field image in an arbitrary relative height H_{rel}. We evaluate the experimental data, plotted in the Fig. 2(d), by changing the H_{rel} in an experimental range from $95\ \mu m$ to $79\ \mu m$, in a step of $2\ \mu m$. The data of the Fig. 2(d) provide a calibration curve for translating the A_{rel}, which is a thing that we can measure by microscopy optical inspection, into the H_{rel} that is fundamental for tracking the dynamic motion of the single-cell. In fact, these data can be nicely fitted to a double exponential, given by:

$$H_{rel} = A_1 * exp\left(-\frac{A_{rel}}{t_1}\right) + \tag{3}$$
$$+ A_2 * exp\left(-\frac{A_{rel}}{t_2}\right) + y0$$

there is no further physical meaning related to the parameters $A_{1(2)}$, $t_{1(2)}$ and $y0$, and they are free to assume arbitrary values to provide the best fit of the (3) to the experimental data. As we can see, the fitting curves are very similar for both systems and it is expected since the calibration curves should not depend on the object under inspection but only dependent on the confocal microscopy apparatus used (such as objective lens, CCD camera, etc).[10]

Fig. 3(a) pictures how to measure the cell density from its dynamics. When the device is on, the single-cell is at an equilibrium position. The second Newton's law can mathematically express this condition in the follow manner

$$\sum \vec{F} = \vec{F}_{Buoyancy} + \vec{F}_{Drag} + \tag{4}$$
$$+ \vec{F}_{Gravity} + \vec{F}_{Acoustic} = 0$$

(4) includes forces such Buoyancy force $\vec{F}_{Buoyancy} (= \frac{4}{3}\pi r^3 \rho_{fluid} \hat{z})$, Stokes drag force $\vec{F}_{Drag} (= 6\pi r \mu v \hat{z})$, gravitational force $\vec{F}_{Gravity} (= -\frac{4}{3}\pi r^3 \rho_{particle} \hat{z})$ and the acoustic radiation force $\vec{F}_{Acoustic} (= -\nabla U^{rad} \hat{z}$, where U^{rad}

is potential acoustic function[6]). The ρ_{fluid}, $\rho_{particle}$ are the density of the fluid and particle, respectively. The r is the radius of the cell, v is its instantaneous velocity of the cell in respect to the fluid and μ is the fluid dynamic viscosity.

On the other hand, as the device is switched off, the acoustic radiation force is removed, and the (4) states that the system is subject to a resulting force downwards, as follows:

$$\sum F = \frac{4}{3}\pi r^3(\rho_{fluid} - \rho_{particle}) + \quad (5)$$
$$+ 6\pi r\mu v = \frac{4}{3}\pi r^3 \rho_{particle}\frac{dv}{dt}$$

The (5) is a simple first order linear differential and its solution for v is given by:

$$v = \frac{2r^2 g(\rho_{fluid}-\rho_{particle})}{9\mu}(1 - e^{-\frac{t}{\tau}}) \quad (5)$$

The $\tau(= \frac{2\rho_{particle}r^2}{6\mu})$ is very small and of the order of microseconds. For that reason, the term $e^{-\frac{t}{\tau}}$, responsible for inertial force, can be neglected. Therefore, the (6) can be written in terms of the rate change of the H_{rel} in respect to time, as mathematically expressed:

$$\frac{dH_{rel}}{dt} = \frac{2r^2 g(\rho_{fluid}-\rho_{particle})}{9\mu} \quad (5)$$

On this dynamic condition, the single-cell starts to fall and we can track its dynamics motion by monitoring the variances of the cell's bright-field images and, with the assistance of the experimental calibration provided by the data in Fig. 2(d) (and the (3)), translate it to the position of the cells as the time goes by.

The data of the dynamics of the scenarios, single-cell (red circles) as well as for polystyrene single-bead (black circles), are displayed in Fig. 3(b). These data are averaged values from 10 measurements under the same conditions, and the deviation is included for each scenario. For both of them, we clearly see a linear tendency of H_{rel} as the time t increases, suggesting that our experimental results can be nicely fitted to the (7), which was derived by simple consideration based on classical mechanics. By doing so, the experimentally obtained values of $\frac{dH_{rel}}{dt}$ for both scenarios, single-cell and polystyrene single-bead. The numerical values of ρ_{fluid}; μ; and g are $997\frac{kg}{m^3}$; $0.89\,mPa\cdot s$; $9.8\frac{m}{s^2}$, respectively. They were used as input values into the (7) to determine $\frac{dH_{rel}}{dt}$ (by the fitting) as well as the density $\rho_{particle}$ (single-cell or polystyrene single-bead).

The density of the macrophage (j774.A1) single-cell was also experimentally determined and the value is of $1040 \pm 21\frac{kg}{m^3}$. This result is in agreement with densities of low-density macrophage range from 1039-1052,[11] although it is from a different macrophage line. The density of the polystyrene single-bead was experimentally calculated to be $1058 \pm 22\ \frac{kg}{m^3}$. This result was very close to that provided by the company that commercialize this material ($\sim 1050\frac{kg}{m^3}$). It is a proof of concept of our methodology of measuring the density of a microparticle because we could determine the density of the single-bead with an accuracy of higher than 99%. The density of the macrophage single-cell was also experimentally determined and the value is of $1040 \pm 21\frac{kg}{m^3}$.

Conclusions

The density of two different systems were experimentally determined using a methodology based on a model of a particle falling in a microfluidic cavity, with no influence of wall's effect, working hand in hand with confocal optical inspection. The reliability of our model used was proved by measuring the density of a commercial polystyrene single-bead ($\sim 1058 \pm 22\ \frac{kg}{m^3}$), which presented a value very close to that provided by the company ($\sim 1050\ \frac{kg}{m^3}$). Using the same methodology and model, the density of the macrophage single-cell (alive murine J774, red dots) was determined to be $1040 \pm 22\ \frac{kg}{m^3}$). This value is in the range of values reported in literature for this cellular model. However, differences might be related to cell culture methodology, experimental conditions, types of culture medium, cellular line, etc.

Acknowledgements

We acknowledge the financial support from Brazilian Agencies: Funding Authority for Studies and Projects FINEP (grants INFRAPESQ-11 and INFRAPESQ-12), Council for Scienti c and Technological Development CNPq (grant numbers 431736/2018-9, 304967/2018-1, 308357/2019-1). H.D.A. Santos thanks the Dimensions Sciences BRIDGES.

References

1. Wu, M., et al., *Acoustofluidic separation of cells and particles.* Microsystems & Nanoengineering, 2019. **5**(1): p. 32.

2. Evander, M. and J. Nilsson, *Acoustofluidics 20: Applications in acoustic trapping.* Lab on a Chip, 2012. **12**(22): p. 4667-4676.

3. Li, S., et al., *Application of an acoustofluidic perfusion bioreactor for cartilage tissue engineering.* Lab on a Chip, 2014. **14**(23): p. 4475-4485.

4. Nasseri, B., et al., *Point-of-care microfluidic devices for pathogen detection.* Biosensors & bioelectronics, 2018. **117**: p. 112-128.

5. Wu, Z., et al., *The acoustofluidic focusing and separation of rare tumor cells using transparent lithium niobate transducers.* Lab on a Chip, 2019. **19**(23): p. 3922-3930.

6. Santos, H.D.A., et al., *3D-Printed Acoustofluidic Devices for Raman Spectroscopy of Cells.* Advanced Engineering Materials. **n/a**(n/a): p. 2100552.

7. Bryan, A.K., et al., *Measurement of mass, density, and volume during the cell cycle of yeast.* Proceedings of the National Academy of Sciences, 2010. **107**(3): p. 999-1004.

8. Yuliang, Z., et al., *Rapid Determination of Cell Mass and Density using Digitally-Controlled Electric Field in a Microfluidic Chip.* Lab on a chip, 2014. **14**.

9. Camacho-Fernández, C., et al., *Comparison of six different methods to calculate cell densities.* Plant Methods, 2018. **14**(1): p. 30.

10. Subbarao, M. and G. Surya, *Depth from defocus: A spatial domain approach.* International Journal of Computer Vision, 1994. **13**(3): p. 271-294.

11. Balestrieri, B., et al., *Phenotypic and Functional Heterogeneity of Low-Density and High-Density Human Lung Macrophages.* Biomedicines, 2021. **9**(5): p. 505.

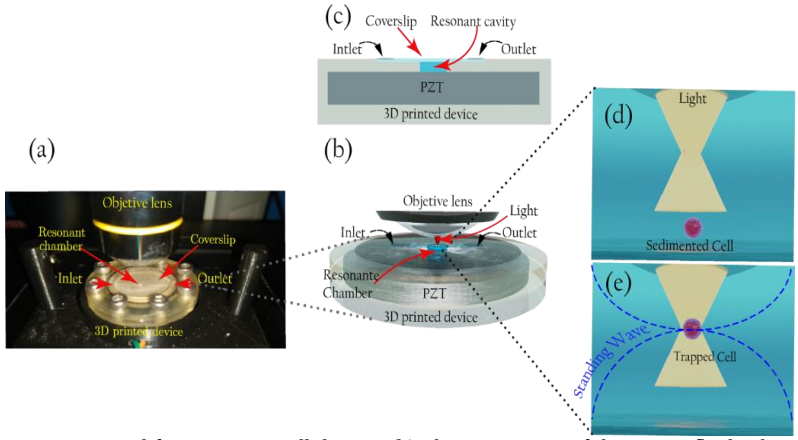

Fig. 1: (a) Optical photo of the system proposed for measuring cell density. (b) The components of the acoustofluidic device are pictured in detail. (c) The cross-section cut view of the device in (b) is also illustrated. (d) When the acoustic wave is off the cell is introduced in the cavity sediments to the bottom. (c) When the acoustic wave is on the cell is trapped in the acoustic levitation plane.

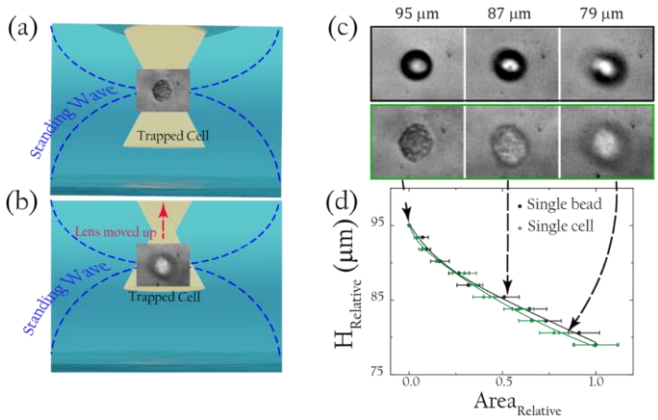

Fig. 2: (a) The light confocal plane matches the acoustic levitation plane. (b) The light confocal plane is moved up in respect to the configuration in (a). (c) Bright-field images of a macrophage single-cell and a polystyrene single-bead are presented in first and second lines, respectively. The bright-field images out of focus are also presented for both systems in the second and third columns. (d) Experimental data of a relative height H_{rel} (defined in equation (1)) as a function of a relative area A_{rel} (defined in equation 2) for both single-cell (green data) and single-bead (black data).

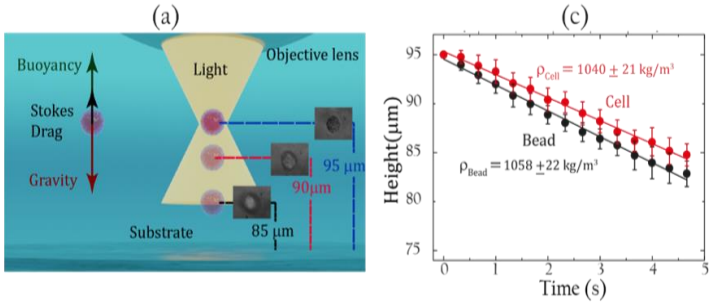

Fig. 2: (a) The light confocal plane matches the acoustic levitation plane. (b) The light confocal plane is moved up in respect to the configuration in (a). (c) Bright-field images of a macrophage single-cell and a polystyrene single-bead are presented in first and second lines, respectively. The bright-field images out of focus are also presented for both systems in the second and third columns. (d) Experimental data of a relative height H_{rel} (defined in equation (1)) as a function of a relative area A_{rel} (defined in equation 2) for both single-cell (green data) and single-bead (black data).